PASJ: Publ. Astron. Soc. Japan **59**, S199–S208, 2007 January 25

Suzaku Observations of HESS J1616−508: Evidence for a Dark Particle Accelerator

Hironori MATSUMOTO,[1] Masaru UENO,[2] Aya BAMBA,[3] Yoshiaki HYODO,[1] Hideyuki MORI,[1]
Hideki UCHIYAMA,[1] Takeshi Go TSURU,[1] Katsuji KOYAMA,[1] Jun KATAOKA,[2] Hideaki KATAGIRI,[4]
Tadayuki TAKAHASHI,[5] Junko HIRAGA,[3] Shigeo YAMAUCHI,[6] John P. HUGHES,[7]
Atsushi SENDA,[3] Motohide KOKUBUN,[8] Takayoshi KOHMURA,[9] and Frederick S. PORTER[10]
[1]*Department of Physics, Graduate School of Science, Kyoto University, Sakyo-ku, Kyoto 606-8502*
matumoto@cr.scphys.kyoto-u.ac.jp
[2]*Department of Physics, Faculty of Science, Tokyo Institute of Technology, 2-12-1 Ookayama, Meguro-ku, Tokyo 152-8551*
[3]*RIKEN, Cosmic radiation group, 2-1 Hirosawa, Wako, Saitama 351-0198*
[4]*Department of Physics, Graduate School of Science, Hiroshima University, 1-3-1 Kagamiyama, Higashi-Hiroshima, Hiroshima 739-8526*
[5]*Institute of Space and Astronautical Science, Japan Aerospace Exploration Agency, 3-1-1 Yoshinodai, Sagamihara, Kanagawa 229-8510*
[6]*Faculty of Humanities and Social Sciences, Iwate University, 3-18-34 Ueda, Morioka, Iwate 020-8550*
[7]*Department of Physics and Astronomy, Rutgers University, 136 Frelinghuysen Road, Piscataway, NJ 08854-8019, USA*
[8]*Department of Physics, The University of Tokyo, 7-3-1 Hongo, Bunkyo-ku, Tokyo 113-0033*
[9]*Department of General Education, Kogakuin University, 2665-1 Nakano-Cho, Hachioji, Tokyo 192-0015*
[10]*NASA Goddard Space Flight Center, Laboratory for High Energy Astrophysics, Code 662, Greenbelt, MD 20771, USA*

(Received 2006 July 28; accepted 2006 August 16)

Abstract

We observed the bright unidentified TeV γ-ray source HESS J1616−508 with the X-ray Imaging Spectrometers onboard the Suzaku satellite. No X-ray counterpart was found to a limiting flux of $3.1 \times 10^{-13}\,\mathrm{erg\,s^{-1}\,cm^{-2}}$ in the 2–10 keV band, which is some 60-times below the γ-ray flux in the 1–10 TeV band. This object is bright in TeV γ-rays, but very dim in the X-ray band, and thus is one of the best examples in the Galaxy of a "dark particle accelerator." We also detected soft thermal emission with $kT \sim 0.3$–0.6 keV near the location of HESS J1616−508. This may be due to a dust-grain scattering halo from the nearby bright supernova remnant RCW 103.

Key words: acceleration of particles — X-rays: individual (HESS J1616−508) — X-rays: ISM

1. Introduction

Since the discovery of cosmic rays, the origin of these high-energy particles has been a mystery. Recent observational studies have revealed that some supernova remnants (SNRs) have non-thermal X-ray emission (e.g., Koyama et al. 1995; Hwang et al. 2002; Bamba et al. 2003b; Vink, Laming 2003; Bamba et al. 2005), which can be interpreted as synchrotron radiation from electrons with energies approaching $E \sim 10^{14}$ eV. TeV γ-rays have also been detected from some of these non-thermal shell-type SNRs. Such very high energy (VHE) gamma-rays have been explained by either (1) Inverse-Compton (IC) upscattering of cosmic microwave background (or other lower frequency) photons by the same high-energy electrons giving rise to the X-ray synchrotron emission or (2) the decay of neutral pions that originate in collisions between high-energy protons and dense interstellar matter (e.g., Pannuti et al. 2003; Lazendic et al. 2004; Katagiri et al. 2005). Thus, the combination of VHE gamma-ray and non-thermal X-ray emission is expected to be a key observational feature of high-energy particle accelerators. A high-sensitivity survey of the galactic plane in VHE γ-rays has been conducted by the High Energy Stereoscopic System (HESS) team, which discovered fourteen new VHE γ-ray sources (Aharonian et al. 2005a, 2006). HESS J1616−508 (hereafter HESS J1616) is one of the brightest of these new sources and, furthermore, is spatially extended with an angular diameter of $\sim 16'$ in the HESS data. Three known objects, the young hard X-ray pulsar PSR J1617−5055, the SNR RCW 103 (G332.4−0.4), and the SNR Kes 32 (G322.4+0.1), are in the vicinity of HESS J1616 ($\sim 10'$–$15'$ away from it), but none provides a convincing identification (Aharonian et al. 2005a, 2006).

Before the HESS galactic plane survey, a few extended γ-ray objects with no clear counterpart in other wavebands had been found. These objects have been denoted "dark particle accelerators" (Aharonian et al. 2005a; Ubertini et al. 2005). They are of interest since they may be indicating the acceleration of nucleons; on the other hand, if the TeV emission comes from electrons, peculiar conditions, such as extremely low magnetic fields, may be necessary, due to the short radiative lifetimes of high-energy electrons (Yamazaki et al. 2006). TeV 2032+410, discovered by the High Energy Gamma-Ray Astronomy (HEGRA) collaboration (Aharonian et al. 2002), was the first object of this kind. In spite of several multi-wavelength follow-up studies, no compelling counterpart has been found from radio to X-ray wavelengths (Mukherjee et al. 2003; Butt et al. 2003, 2006). HESS J1303−631 is another example (Aharonian et al. 2004a). Mukherjee et al. (2003) observed this target with the Chandra X-ray Observatory for 5 ks, and placed an upper limit of $< 5.4 \times 10^{-12}\,\mathrm{erg\,s^{-1}\,cm^{-2}}$ to its diffuse hard X-ray flux in the 2–10 keV band.

HESS J1616 is brighter than both TeV 2032+410 and

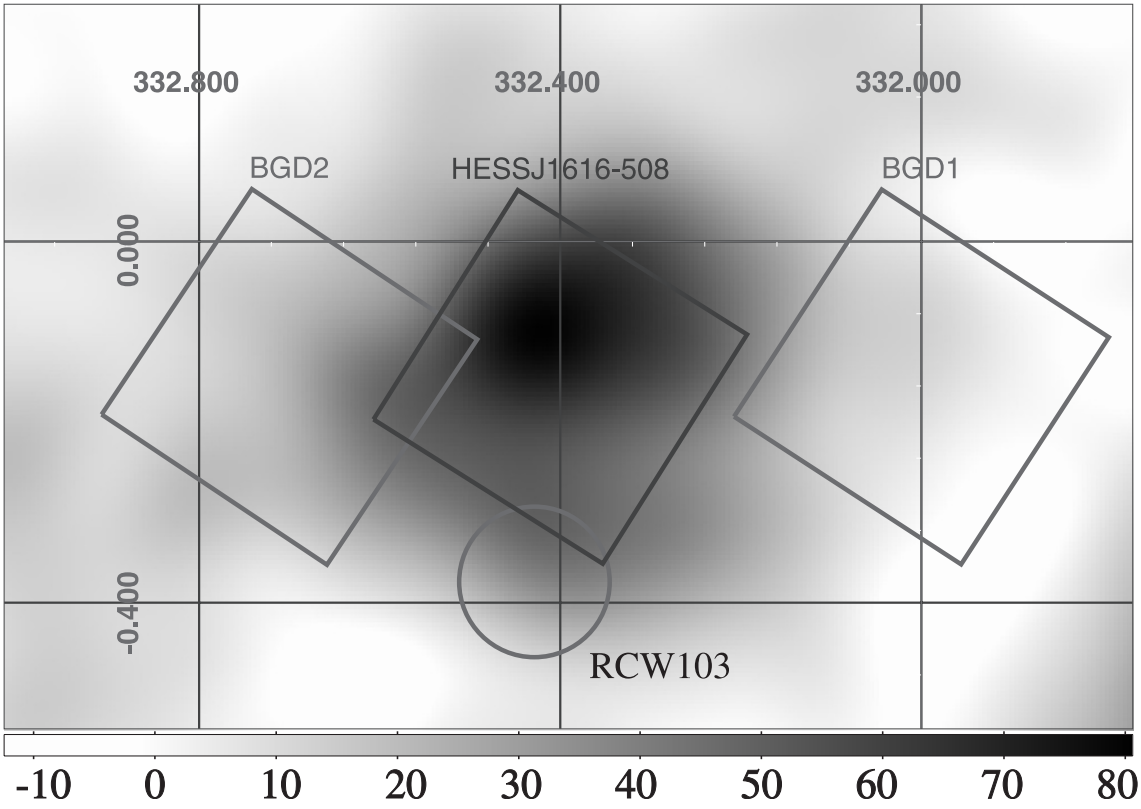

Fig. 1. Suzaku field of view overlaid on the HESS smoothed excess map in galactic coordinates (axis labels are in degrees). The circle shows the position and approximate size of RCW 103, which is the nearest X-ray bright SNR. The scale bar below the figure shows the excess.

HESS J1303−631 in the TeV regime (see also table 3) and is therefore a more suitable case for examining if dark accelerators really exist and for finding out just how "dark" they are. Since many VHE γ-ray objects are X-ray emitters, the X-ray band is the natural place to search for a counterpart. To date there have been no X-ray observations explicitly targeting HESS J1616, so we observed HESS J1616 with the Suzaku satellite (Mitsuda et al. 2007). The Suzaku X-ray Imaging Spectrometer (XIS) (Koyama et al. 2007), with their high sensitivity and stable low background (Yamaguchi et al. 2006), are optimal devices to search for diffuse X-ray emission. This is especially the case in the hard X-ray band ($E \gtrsim 6$ keV), where non-thermal emission dominates over thermal, and the effects of X-ray absorption are minimized. By detecting, or even just setting a sensitive upper limit on the X-ray emission from HESS J1616, it should be possible to address the question of what types of particles, electrons or protons, are accelerated in the object, and to constrain the acceleration mechanism by comparing the X-ray and γ-ray emission. In addition to the Suzaku data, we also used XMM-Newton archival data that partly covered the HESS J1616 region. In this work, uncertainties are quoted at the 90% confidence level unless otherwise stated.

2. Observations and Data Reduction

The center of HESS J1616 was observed on 2005 September 19 during the Science Working Group (SWG) phase program. We also observed two nearby positions with the same galactic latitude (BGD 1 and BGD 2 in figure 1). These positions were chosen so that no known bright X-ray sources fell in the field of view and were close enough to HESS J1616 that the brightness of the galactic ridge X-ray emission (e.g. Worrall et al. 1982; Koyama et al. 1986; Yamauchi, Koyama 1993; Sugizaki et al. 2001; Revnivtsev et al. 2006) could be estimated accurately at the source position. The observations are summarized in table 1.

The observations were made with four CCD cameras (designated as XIS 0–3: Koyama et al. 2007) at the foci of four X-ray telescope (XRT: Serlemitsos et al. 2007), and a hard X-ray detector (HXD: Kokubun et al. 2007; Takahashi et al. 2007). Since the hard X-ray source PSR J1617−5055 (Torii et al. 1998) is in the HXD field of view, we concentrate on the XIS data.

The XIS was operated in the normal clocking mode during all three observations. The edit mode was 3×3 or 5×5 for the HESS J1616 field, and we combined the data of both modes for our analysis, while only the 3×3 mode was used in the background pointings. We used the HEADAS software version 6.0.4 and version 0.7 of the processed data.[1] Data affected by the South Atlantic Anomaly, Earth occultation, and telemetry

[1] Version 0.7 processing is an internal processing applied to the Suzaku data obtained during the SWG phase, for the purpose of establishing the detector calibration as quickly as possible. Official data distributed to guest observers are processed Version 1.0 or higher. See Mitsuda et al. (2007) and Fujimoto et al. (2007) for more details.

Table 1. Log of Suzaku observations.

Name	Position (degree)		Start time	End time	Effective exposure (ks)			
	l	b			XIS 0	XIS 1	XIS 2	XIS 3
HESS J1616	332.400	−0.150	2005/9/19 12:09:58	2005/9/20 19:37:50	45.0	45.4	45.0	45.0
BGD 1	332.000	−0.150	2005/9/18 22:56:14	2005/9/19 10:59:02	21.1	23.7	21.2	21.7
BGD 2	332.700	−0.150	2005/9/20 19:37:50	2005/9/21 07:28:46	23.5	23.7	23.5	23.5

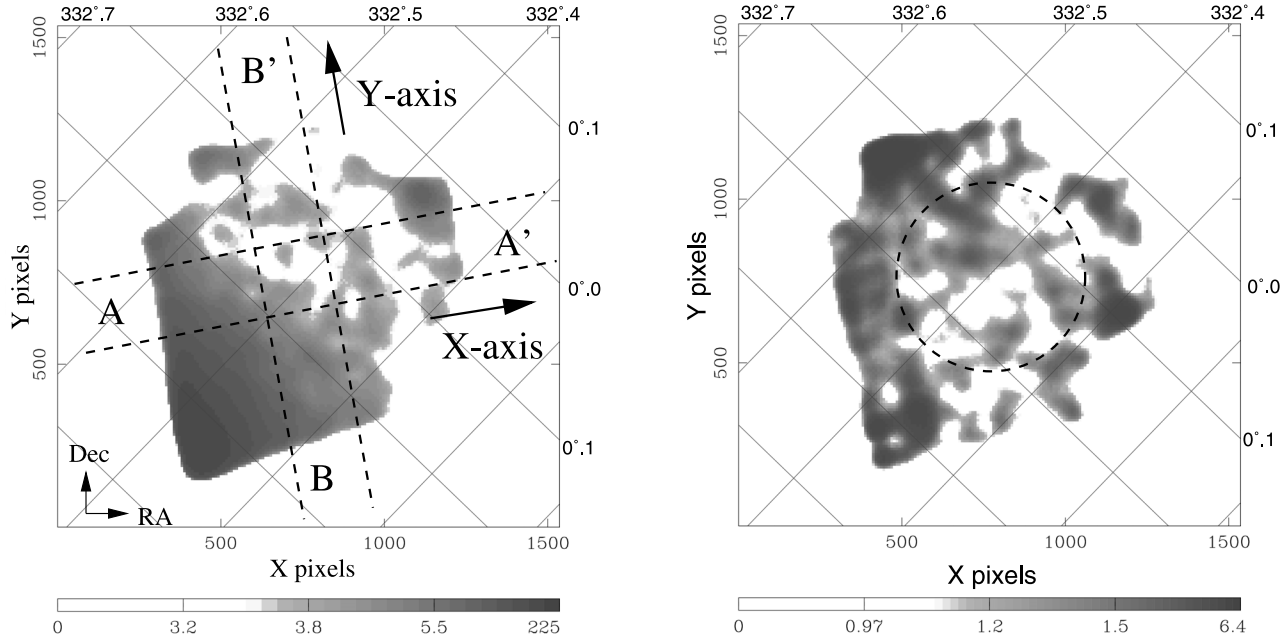

Fig. 2. Suzaku XIS images of the HESS J1616 field in the soft (left: 0.6–3 keV) and hard (right: 3–12 keV) energy bands. Lines of constant galactic latitude and longitude are plotted. The scale bars under the figures show the photon count. The images were smoothed using a Gaussian function with a sigma of 0′.42. Vignetting correction was applied after subtracting non-X-ray backgrounds, as described in the text. The dotted lines in the left figure show the regions used for the photon-count profiles shown in figure 3. The dotted circle with a radius of 5′ in the right figure shows the region where we extracted the XIS spectra.

saturation were excluded. Hot and flickering pixels were also removed. We did not screen the data with the elevation angle from the bright Earth in order to maximize the statistics in the hard X-ray band; more than 99% of the contamination from the bright Earth consists of the O Kα and N Kα lines originating in the atmosphere, and the data above 0.6 keV are not affected by the contamination. In the following analysis we use the XIS data from 0.6 keV to 12 keV. After data screening, the effective exposures were 45 ks, 21 ks, and 24 ks for the HESS J1616, BGD 1, and BGD 2 regions, respectively.

3. Analysis and Results

3.1. XIS Image

We concentrate on the front-illuminated (FI) CCD data in this imaging analysis, since non-X-ray background (NXB) dominates the data of the back-illuminated (BI) CCD (XIS1) in the high-energy band, especially above 8 keV. In figure 2, XIS images of the HESS J1616 region are shown for the soft (0.6–3.0 keV) and hard (3.0–12.0 keV) energy bands. We excluded the corners of the chips that were illuminated by the ^{55}Fe calibration sources, and images from the three FI CCDs (XIS 0, XIS 2, and XIS 3) were summed. Images of the NXB were constructed from night Earth data provided by the XIS team and subtracted from the HESS J1616 images. After NXB subtraction, vignetting corrections were done as follows. We produced simulated XIS images assuming a uniform surface brightness, using the XRT + XIS simulator `xissim` ver. 2006-05-28 (Ishisaki et al. 2007). We assumed monochromatic X-rays of energy 1.49 or 8.05 keV, where the vignetting function is best calibrated (Serlemitsos et al. 2007). The simulated images were normalized so that pixels at the optical axis had values of ~ 1. We divided the soft and hard HESS J1616 images by the simulated 1.49 and 8.05 keV images. Finally, the resulting images were rebinned by a factor of 8 and smoothed using a Gaussian function with a sigma of 0′.42.

Since the lower left corner of the field of view marginally overlaps the bright SNR RCW 103, corresponding bright emission can be seen in the soft band image. On the other hand, there is no such structure in the hard band image. Furthermore, there is no apparent X-ray structure suggesting an X-ray counterpart of HESS J1616 both in the soft and hard band images. To examine this more quantitatively, we made

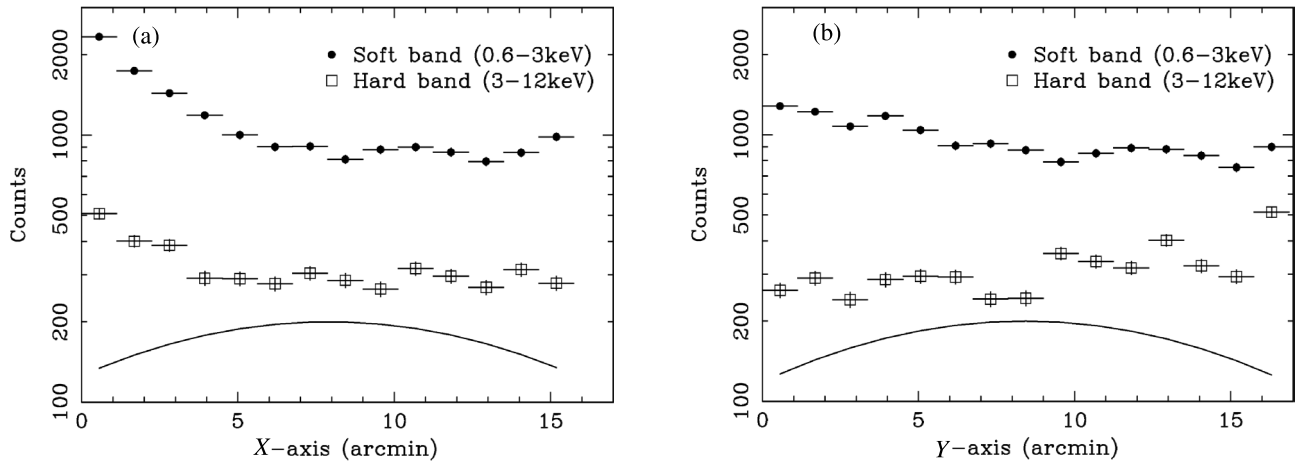

Fig. 3. Photon count profiles of the XIS images along the strips AA′ (a) and BB′ (b) shown in figure 2. The errors are estimated at the 1σ confidence level. The curve in the figures shows the Gaussian function of $\sigma = 8'.2$, which expresses the TeV γ-ray profile of HESS J1616.

photon count profiles along the strips AA′ and BB′ with a width of 4′.2 in figure 2; the profiles are shown in figure 3.

In the soft energy band, the photon count gradually decreases along both the X and Y axes, which shows the influence of RCW 103. A similar trend can be seen even in the hard energy band along the X axis, but we do not see it along the Y axis. The trend in the hard energy band may have a different origin from the soft band profile; the hard X-ray pulsar PSR J1617−5055 or fluctuations of the galactic ridge emission may explain the hard band profile. We see no systematic trend in either the hard or soft X-ray profiles consistent with the TeV γ-ray profile of HESS J1616, which can be described by a Gaussian function with $\sigma = 8'.2$ (Aharonian et al. 2006). In summary, according to our imaging analysis, there is no apparent X-ray counterpart to HESS J1616.

3.2. *XIS Spectrum*

We made the XIS spectrum of the HESS J1616 region from each XIS sensor by extracting X-ray events from within a 5′ radius of the center of the field of view. We also tried to extract spectra for the BGD 1 and BGD 2 regions in the same way as for the HESS J1616 region, but we discovered several X-ray sources in the extraction regions; there is an X-ray object in the BGD 1 region (designated Suzaku J1614−5114) at $(l, b) = (331.^\circ98, -0.^\circ22)$, and two X-ray sources are found in the BGD 2 region at $(l, b) = (332.^\circ67, -0.^\circ19)$ and $(332.^\circ77, -0.^\circ20)$ (designated Suzaku J1617−5044 and Suzaku J1618−5040, respectively). According to the SIMBAD Astronomical Database operated at CDS, Strasbourg, France,[2] Suzaku J1614−5114 and Suzaku J1618−5040 are positionally coincident with the B-type star CD−50 10270 and the infrared source IRAS 16145−5033, respectively. We were unable to identify the counterpart to Suzaku J1617−5044. We excluded these sources from the BGD 1 and BGD 2 spectra using 2′ radius circular regions. The spectra from the FI CCDs were combined after extraction.

These spectra contain the NXB. For the most accurate NXB estimate, we filtered the night Earth data so that the cut-off rigidity distribution was the same for the HESS J1616, BGD 1 and BGD 2 spectra (Koyama et al. 2007), and extracted the NXB spectra using the same regions in detector coordinates (DETX/Y). The thus-made NXB spectra were subtracted from the HESS J1616, BGD 1, and BGD 2 spectra; the resulting spectra are plotted in figure 4, where the BGD 1 and BGD 2 spectra are renormalized to compensate for the difference in the area of the spectral extraction regions.

Figure 5 is the ratio of the spectrum of the HESS J1616 region to those of the background regions. The ratio is larger than unity below 4 keV, while it is close to unity in the 4–8 keV band. The ratio becomes noisy above 8 keV, where the NXB dominates the high-energy band.

The most likely origin for the soft band excess in the HESS J1616 region is the nearby SNR RCW 103. Here, we consider whether instrumental effects, i.e., the tail of the point spread function (PSF) and stray light of the XRT, might be the cause. The HESS J1616 region spectrum exhibits emission lines at 0.83 keV, 0.92 keV, 1.02 keV, and 1.35 keV, which are attributed to Fe XVII, Ne IX, Ne X, and Mg XI, respectively, and strongly indicate thermal plasma emission. This type of soft spectrum resembles that of RCW 103. Using `xissim` we simulated how many photons would fall into the HESS J1616 region from RCW 103, which has a radius of $\sim 5'$ and is centered 13′ from the HESS J1616 region. In the simulation, we employed a nonequilibrium ionization plasma model with temperature $kT = 0.3$ keV, column density $N_{\rm H} = 7 \times 10^{21}\,{\rm cm}^{-2}$, and ionization parameter $nt = 6 \times 10^3\,{\rm cm}^{-3}\,{\rm yr}$ for the spectrum of RCW 103 (Gotthelf et al. 1997). As for the metal abundances, we set them to 0.5-times the cosmic values (Anders, Grevesse 1989). The flux of RCW 103 was set to $1.8 \times 10^{-10}\,{\rm erg\,s^{-1}\,cm^{-2}}$ in the 0.6–2.0 keV band (Tuohy, Garmire 1980) and the Chandra ACIS image of RCW 103 (from ObsID 123) was used as the input surface brightness distribution. The simulation predicted count rates of $1.6 \times 10^{-3}\,{\rm c\,s^{-1}}$ (FI) and $2.4 \times 10^{-3}\,{\rm c\,s^{-1}}$ (BI) in the 0.6–2.0 keV band. The measured FI count rate from the HESS J1616 spectrum is $4.6 \times 10^{-2}\,{\rm c\,s^{-1}}$ with an error of $\pm 0.1 \times 10^{-2}\,{\rm c\,s^{-1}}$

[2] ⟨http://simbad.u-strasbg.fr/Simbad/⟩.

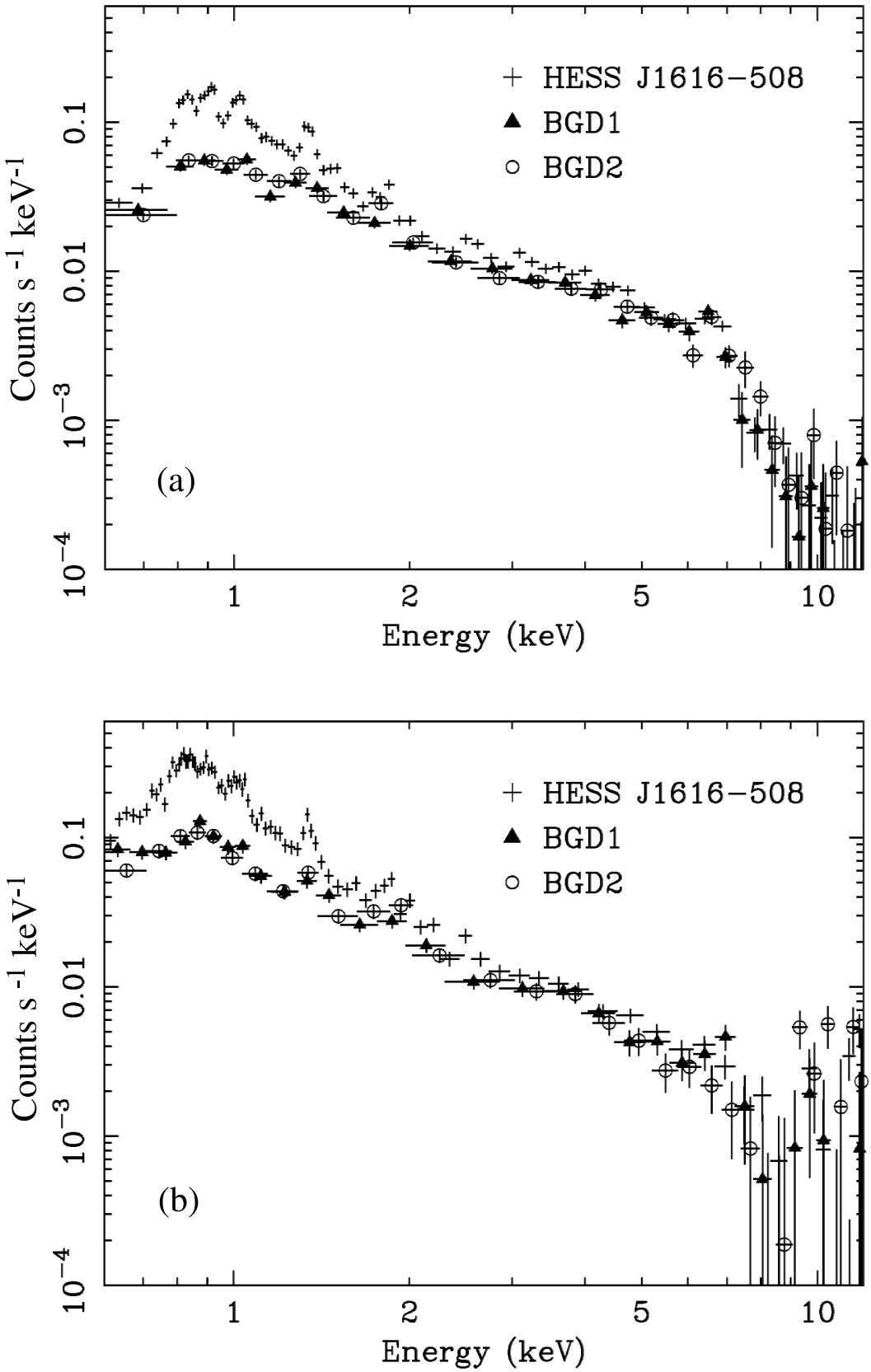

Fig. 4. XIS spectra from the HESS J1616, BGD 1, and BGD 2 regions: (a) combined FI spectra (XIS 0 + XIS 2 + XIS 3), and (b) BI spectra (XIS 1). Non-X-ray backgrounds were subtracted as described in the text. Error bars on the data points are plotted at the 1σ confidence level.

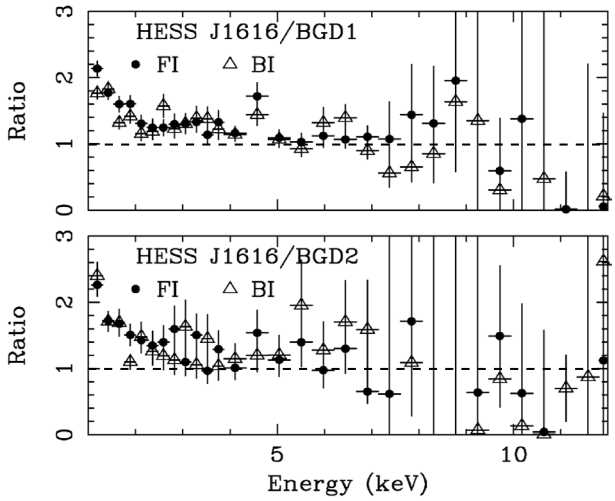

Fig. 5. Ratio of the spectra shown in figure 4. Errors on the data points are 1σ.

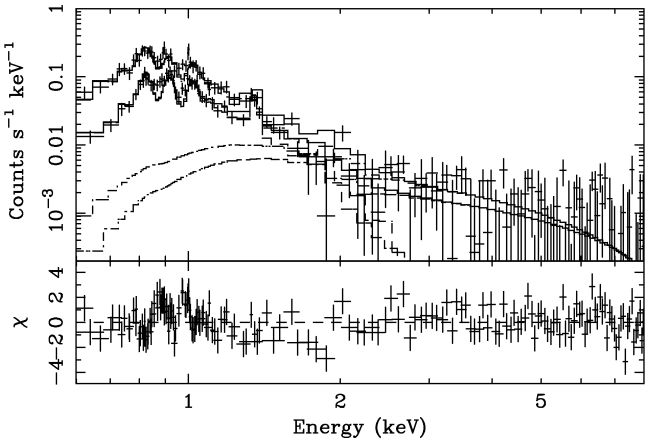

Fig. 6. HESS J1616 spectra of the FI and BI CCDs with the best-fit model. The BGD 2 data were used for background subtraction.

Table 2. Best-fit parameters for the model fitting.

Background*	BGD 1	BGD 2
$N_{\rm H}$ (10^{21} cm^{-2})	$1.68^{+0.47}_{-0.49}$	$4.13^{+0.45}_{-0.45}$
kT (keV)	$0.59^{+0.019}_{-0.017}$	$0.30^{+0.018}_{-0.015}$
Abundance (cosmic)	0.50 (fixed)	0.50 (fixed)
$f_{\rm x}^{\rm APEC}$ (0.6–2 keV)†	7.05×10^{-13}	7.55×10^{-13}
Γ‡	2.0 (fixed)	2.0 (fixed)
Normalization (10^{-5})§	$7.74^{+2.73}_{-2.83}$	$9.00^{+2.88}_{-2.92}$
$\chi^2/d.o.f.$	273.11/232	276.45/232

* Data used for background in the spectral fitting.
† Flux (erg s^{-1} cm^{-2}) of the APEC model in the 0.6–2 keV band (uncorrected for absorption).
‡ Photon index of the power-law model.
§ Normalization of the power-law model defined as the differential photon number flux (i.e., photons keV^{-1} s^{-1} cm^{-2}) at 1 keV. Errors are quoted at the 99% confidence level.

depending on the background data set used. The BI count rate is 9.4×10^{-2} c s^{-1} with the same uncertainty. These are more than a factor of 10 *higher* than predicted from the instrumental effects alone, suggesting that the observed soft emission in the HESS J1616 region may have an astrophysical origin. However, the current calibrations of the PSF tail and stray light at large off-axis angles have large systematic errors. A more detailed understanding of the XRT will be needed before drawing more definitive conclusions about the putative soft emission, and that is beyond the scope of this paper.

Since the spectral ratio becomes noisy above 8 keV, we examined the ratio of HESS J1616 to BGDs from 4 to 8 keV. The average of the ratio and its 99% confidence range is found to be $1.10^{+0.11}_{-0.11}$ and $1.07^{+0.12}_{-0.11}$ in the cases of HESS J1616/BGD 1 and HESS J1616/BGD 2, respectively. Thus we cannot conclude a positive detection of hard X-ray emission from HESS J1616 at the 99% confidence level with the current statistics of the Suzaku XIS data.

Next, we proceed to the spectral fitting. Both the FI and BI spectra of the HESS J1616 region in the 0.6–8 keV band, from which either BGD 1 or BGD 2 were used for the background subtraction, were fitted simultaneously. To describe the putative soft X-ray emission, we used a thermal plasma model (the APEC model: Smith et al. 2001), and we added a power-law model to quantify any hard X-ray emission from the HESS J1616 region. Both components were modified by the same interstellar absorption. In the spectral fitting, we used standard RMFs and we made ARFs for a flat sky distribution with the software `xissimarfgen` ver. 2006-05-28 (Ishisaki et al. 2007). Quoted values for fluxes and normalizations in the following are normalized to correspond to a uniform sky distribution over a $5'$ radius. The best-fit parameters are summarized in table 2, and an example of the best-fitted spectra are shown in figure 6. Note that in the spectral fits the power-law component is always statistically significant, even at the 99% confidence level, although it is mainly required to fit the spectra in the 2–4 keV band. This energy range includes the soft excess discussed above, which may be related to RCW 103. If we replace the power-law model by a second thermal component, we obtain fits with similar goodness of fit. For example, in the case of the BGD 2-subtracted spectra, temperatures of $kT = 0.62$ keV and $kT = 2.0$ keV plasma with the same metallicity of 0.5 times cosmic abundance and $N_{\rm H} = 3.5 \times 10^{20}$ cm^{-2} can fit the spectra with $\chi^2/d.o.f. = 265.50/237$. The 2.0 keV thermal component, which may represent contamination from RCW 103 or be part of the putative soft emission, emits 82% of its energy flux in the 0.6–2 keV band. Thus, the significant detection of a hard power-law component does not necessarily demonstrate the existence of hard X-ray emission from HESS J1616. Given the uncertainties associated with the soft diffuse excess, we use the power-law component as a conservative upper limit to the hard X-ray emission. Furthermore, the BGD 2-subtracted case gives the larger value, and so we take this as the upper limit on the normalization of the power-law component. Our upper limit at the 99% confidence level to the unabsorbed flux in the 2–10 keV band of HESS J1616 is 3.1×10^{-13} erg s^{-1} cm^{-2}.

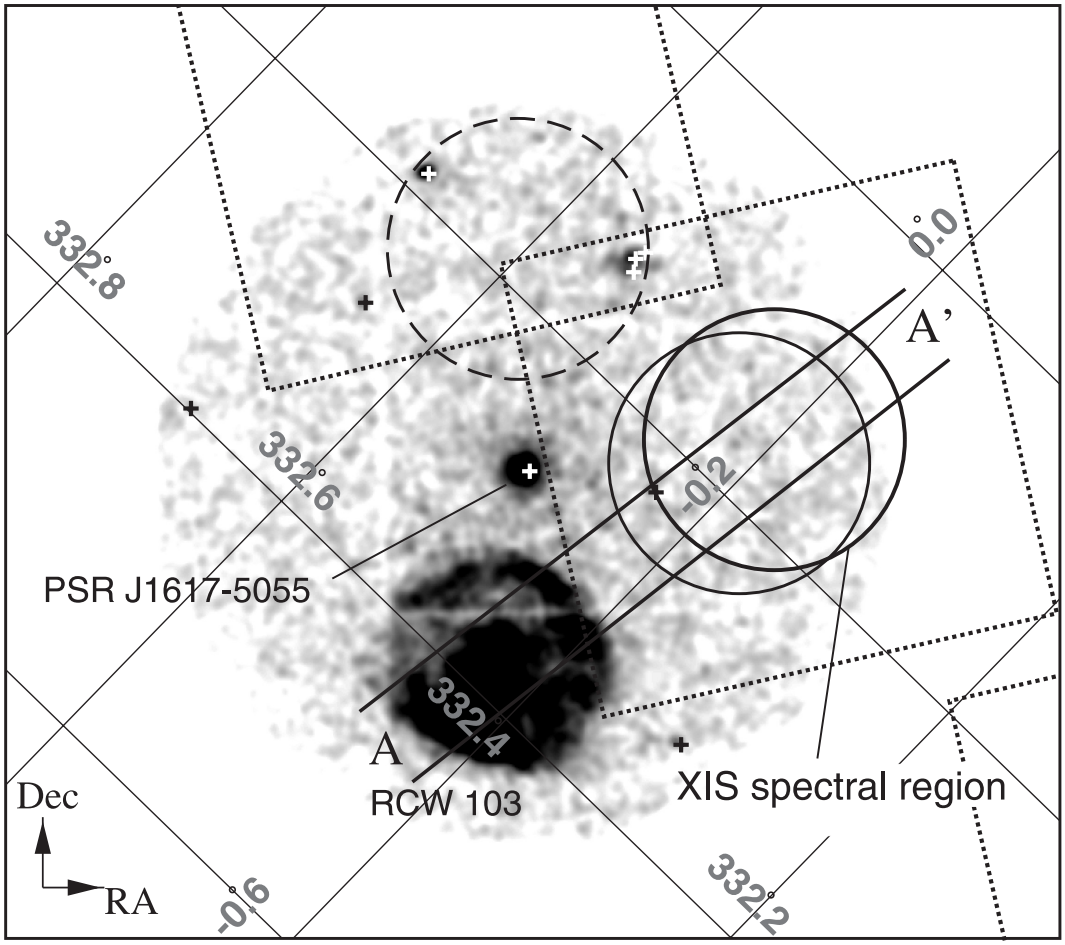

Fig. 7. MOS 1 + 2 2.0–7.0 keV image smoothed with a Gaussian kernel of $\sigma = 10''$. Lines of constant galactic latitude and longitude are plotted and labeled in the interior of the figure. Plotted are the FOVs of the XIS observations (dashed-line squares), the XIS spectral region (thick circle), detected point sources (plus marks), and the source and background spectral regions (solid and dashed thin circles, respectively). Projection profile in figure 8 is made along the strip AA′.

3.3. XMM-Newton Analysis

XMM-Newton (Aschenbach et al. 2000) pointed at the X-ray pulsar, PSR J1617−5055, on 2001 September 3 (ObsID: 0113050701), and this observation partly covered the HESS J1616 region with the EPIC instrument (Strüder et al. 2001; Turner et al. 2001). We also analyzed the XMM-Newton data to check for consistency with the Suzaku results.

The pn camera was operated in the timing mode during this observation, and the data had no imaging information. On the other hand, the MOS 1 and MOS 2 cameras were operated in the standard full-frame mode using the medium filter. We therefore analyzed only the MOS data. We used the Standard Analysis System (SAS) software version 6.0.5 for event selection. From the detected MOS events, we selected those with PATTERN keywords between 0 and 12 as valid X-ray events. Time intervals of high and flaring background were rejected by removing times when the 10–12 keV count rate was higher than $0.15\,\mathrm{c\,s^{-1}}$ in the full field of view. The resultant exposure time was 13 ks for each MOS camera.

Figure 7 shows the combined MOS 1 and MOS 2 image in the 2.0–7.0 keV band. We see no significant excess emission at the position of HESS J1616. Because of its higher spatial resolution, the EPIC observation is more sensitive to point sources than the XIS observation even given the shorter exposure time. We therefore searched for X-ray point sources in the combined MOS 1 + MOS 2 2.0–7.0 keV image using `emldetect` in the SAS software package. In the `emldetect` software, the source significance was determined by comparing the numbers of photons in 68% encircled energy regions to those in the background map, which was prepared using the `esplinemap` software. The likelihood limit was taken to be 10, corresponding roughly to 4σ detection. The detected point sources, excluding those within RCW 103, are shown with plus marks in figure 7. Only one point source was detected at the edge of the XIS spectral region for HESS J1616, but its flux in the 2–10 keV band is $2.2 \times 10^{-14}\,\mathrm{erg\,s^{-1}\,cm^{-2}}$, which is smaller than the XIS upper limit for the hard X-ray emission from HESS J1616 by more than a factor of 10. A source was also found at around the center of the BGD 2 region, but we had already excluded it from the XIS analysis as Suzaku J1617−5044.

The detection limit, S_{lim}, in the 2–10 keV band of this search for point sources at the 4σ confidence level was calculated

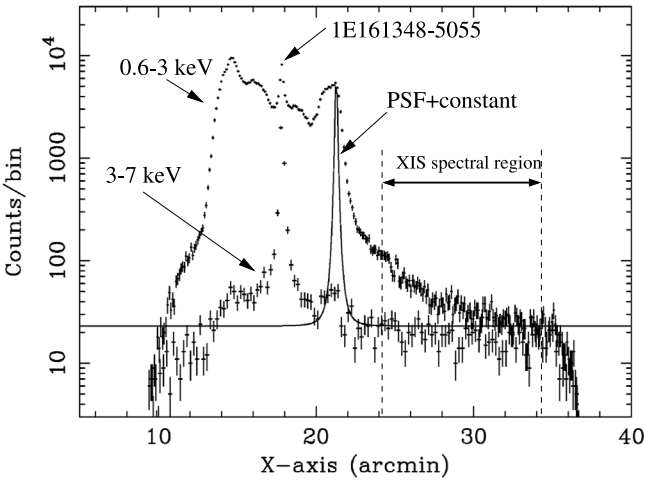

Fig. 8. MOS 1 + 2 projection profiles in the 0.6–3 keV and 3–7 keV bands along the strip AA′ in figure 7.

using the formula $S_{\rm lim} \leq \left(4r\sqrt{\pi b}\,\right)/(0.68\,fT)$, where b is the surface brightness of the background map, r is the radius of the 68% encircled region, f is a counts-to-flux conversion factor (ECF) of $3.8 \times 10^{10}\,{\rm c\,cm^{-2}\,erg^{-1}}$, and T is the "effective" exposure-time corrected for the vignetting. For point sources, we obtained $S_{\rm lim} = 2 \times 10^{-14}\,{\rm erg\,s^{-1}\,cm^{-2}}$ at the center of the XMM field of view, while at the center of the XIS field of view, which is $\sim 9'$ away from the optical axis, $S_{\rm lim} = 3 \times 10^{-14}\,{\rm erg\,s^{-1}\,cm^{-2}}$.

We made photon count profiles along the strip AA′ in figure 7 in the 0.6–3 keV and 3–7 keV band (figure 8). Note that NXB subtraction and vignetting corrections were not applied to the profile. As a reference, we also plot the PSF[3] at the position of the RCW 103 rim ($\sim 6'$ away from the optical axis) plus constant profile in the figure. The difference between the soft and hard band profiles shows an extended soft X-ray halo surrounding RCW 103, qualitatively supporting the soft excess seen in the Suzaku data.

We also searched for larger scale X-ray emission at the position of HESS J1616 in the EPIC data. Source and background spectra were extracted from the circular regions ($5'$ radii) shown in figure 7 (the solid and dashed thin circles, respectively). The background region was chosen to be at the same galactic latitude as the source region so that differences in galactic diffuse emission (Kaneda et al. 1997) would be minimized. The point sources detected in the source and background region were excluded with $2''$ radius circles. MOS 1 and MOS 2 spectra were co-added. To avoid any influence of the putative soft emission, we ignored the data below 3 keV and fitted the spectrum in the 3–7 keV band with a power-law model of a photon index $\Gamma = 2$. The 99% confidence limit on the power-law normalization is $< 2.66 \times 10^{-4}$. The XMM-Newton data thus set an upper limit of $6.9 \times 10^{-13}\,{\rm erg\,s^{-1}\,cm^{-2}}$ on the flux of the hard X-ray emission from HESS J1616 in the 2–10 keV band. This upper limit is two-times larger than the Suzaku result.

[3] In XMM-SOC-CAL-TN-0022 at ⟨http://xmm.esac.esa.int/external/xmm_sw_cal/calib/documentation/index.shtml#XRT⟩.

4. Discussion

Neither the Suzaku nor the XMM-Newton data provide evidence for hard X-ray emission from HESS J1616; the XIS sets the most stringent upper limit of $3.1 \times 10^{-13}\,{\rm erg\,s^{-1}\,cm^{-2}}$ in the 2–10 keV band. The differential photon flux in the TeV γ-ray regime can be represented by a power-law of photon index of $\Gamma = 2.35$ with a total photon flux of $(43.3 \pm 2.0) \times 10^{-12}\,{\rm cm^{-2}\,s^{-1}}$ above 200 GeV (Aharonian et al. 2006). This corresponds to an energy flux of $1.7 \times 10^{-11}\,{\rm erg\,s^{-1}\,cm^{-2}}$ in the 1–10 TeV band. The ratio of the TeV γ-ray flux to the X-ray flux ($f_{\rm TeV}/f_{\rm X}$) is therefore more than ~ 55. Table 3 is a list of spatially extended VHE objects with X-ray observations that we extracted from the H.E.S.S. source catalog.[4] We also added TeV J2032 + 4130 (Aharonian et al. 2002) to the list. Although recent Swift observations found possible counterparts of HESS 1614−518 and HESS J1834−087 (Landi et al. 2006), we do not include them in table 3, since their X-ray data are not statistically enough for spectroscopy. Note that the X-ray counterparts in the list are not secure. For example, AX J1838.0−0655 is the most promising candidate counterpart of HESS J1837−069 (Aharonian et al. 2005a, 2006), but it is slightly outside of the HESS source extension (Landi et al. 2006). HESS J1616 has the most stringent X-ray flux upper limit among the VHE objects; yet of more import is its extremely large flux ratio, $f_{\rm TeV}/f_{\rm X}$, compared to the others. Evidently HESS J1616 is a very peculiar object. The bright TeV γ-ray emission strongly suggests the presence of some particle acceleration processes there; however HESS J1616 emits little X-ray (or lower frequency radiation) emission and thus remained undiscovered prior to the HESS survey. HESS J1616 is thus a strong candidate for being a "dark particle accelerator."

Assuming the origin of the TeV γ-rays to be IC scattering of the cosmic microwave background by accelerated electrons, we can calculate the synchrotron emission from these electrons assuming magnetic field values of B = 10, 1, and 0.1 μG (figure 9). The Suzaku flux limit requires that the magnetic field in HESS J1616 be less than a few microgauss, which is the typical interstellar value, and far below the estimated magnetic field values in other HESS sources, such as RX J0852−4622 and RX J1713.7−3946. Thus, other mechanisms for the TeV emission may be required. Aharonian et al. (2006) proposed an asymmetric undetected pulsar wind nebula (PWN) powered by the young pulsar PSR J1617−505, which is $\sim 13'$ away from HESS J1616, to explain the TeV emission. The spin-down luminosity of PSR J1617−505 is $1.6 \times 10^{37}\,{\rm erg\,s^{-1}}$ (Torii et al. 1998), and in this case the luminosity of the PWN is expected to be $\sim 10^{34}\,{\rm erg\,s^{-1}}$ (Cheng et al. 2004) in the 2–10 keV band. Assuming the pulsar distance to be 3.3 kpc (Torii et al. 1998), we obtain an unabsorbed flux of $7.6 \times 10^{-12}\,{\rm erg\,s^{-1}\,cm^{-2}}$ in the 2–10 keV band. To reconcile this high flux and the XIS upper limit, we would need an absorption of $N_{\rm H} > 2 \times 10^{24}\,{\rm cm^{-2}}$ for a photon index of 2. Since the column density is more than 10-times the absorption to the galactic center (Baganoff et al. 2003), this seems to be an unlikely scenario to explain X and TeV emission. The high $f_{\rm TeV}/f_{\rm X}$ ratio might be explained if

[4] ⟨http://www.mpi-hd.mpg.de/hfm/HESS/public/HESS_catalog.htm⟩.

Table 3. Spatially extended VHE objects with X-ray observations.

Name	Possible counterpart	Type*	$\Gamma_{\rm TeV}$†	$f_{\rm TeV}$‡	$N_{\rm H}$§	$\Gamma_{\rm X}$‖	$f_{\rm X}$#	$f_{\rm TeV}/f_{\rm X}$	References**
HESS J0852−463	RX J0852−4622	SNR	2.1	6.9	4	2.6	~ 10	~ 0.7	1, 2, 3
HESS J1303−631	···	?	2.4	1.0	20	2.0	< 0.64	> 1.6	4, 5
HESS J1514−591	PSR B1509−58	PWN	2.3	1.6	8.6	2.0	3.2	0.5	6, 7
HESS J1632−478	AX J1631.9−4752	HMXB?	2.1	1.7	210	1.6	1.7	1.0	8, 9
HESS J1640−465	G338.3−0.0	SNR	2.4	0.71	96	3.0	0.30	2.4	8, 10
HESS J1713−397	RX J1713.7−3946	SNR	2.2	3.5	8	2.4	54	0.065	11, 12
HESS J1804−216	Suzaku J1804−2142	?	2.7	1.0	2	−0.3	0.025	40	8, 13
HESS J1804−216	Suzaku J1804−2140	?	2.7	1.0	110	1.7	0.043	23	8, 13
HESS J1813−178	AX J1813−178	?	2.1	0.89	110	1.8	0.70	1.3	8, 14
HESS J1837−069	AX J1838.0−0655	?	2.3	1.4	40	0.8	1.3	1.1	8, 15
TeV J2032+4130	···	?	1.9	0.20	?	?	< 0.20	> 1.0	16
HESS J1616−508	···	?	2.4	1.7	4.1	2.0	< 0.031	> 55	This work

* SNR = supernova remnant, PWN = pulsar wind nebula, HMXB = high mass X-ray binary.
† Photon index of TeV spectra.
‡ Unabsorbed flux in the 1–10 TeV band (in $10^{-11}\,{\rm erg\,s^{-1}\,cm^{-2}}$).
§ Column density for X-ray spectra (in $10^{21}\,{\rm cm^{-2}}$).
‖ Photon index of X-ray spectra.
Unabsorbed flux in the 2–10 keV band (in $10^{-11}\,{\rm erg\,s^{-1}\,cm^{-2}}$).
** (1) Aharonian et al. (2005c), (2) Slane et al. (2001), (3) our analysis of the ASCA archival data, (4) Aharonian et al. (2004a), (5) Mukherjee, Halpern (2005), (6) Aharonian et al. (2005b), (7) DeLaney et al. (2006), (8) Aharonian et al. (2006), (9) Rodriguez et al. (2003), (10) Sugizaki et al. (2001), (11) Aharonian et al. (2004b), (12) Slane et al. (1999), (13) Bamba et al. (2007), (14) Brogan et al. (2005), (15) Bamba et al. (2003a), and (16) Aharonian et al. (2002).

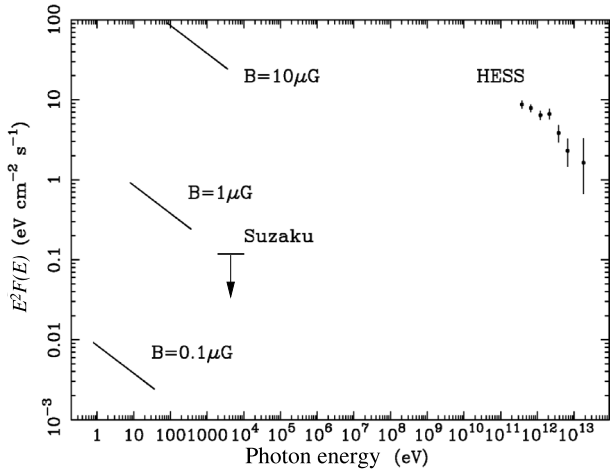

Fig. 9. Spectral energy distribution of HESS J1616 from the X-ray to TeV γ-ray bands. The synchrotron radiation from accelerated electrons, which boost the 3 K background up to the TeV energy range, is plotted toward the left for three different values of the magnetic field.

HESS J1616 is an old SNR, since TeV and X-ray emissions are dominated by hadronic processes and synchrotron radiation from secondary electrons, respectively (Yamazaki et al. 2006). In any case, it remains highly desirable to obtain detailed data of the HESS J1616 region at other wavelengths, especially the radio band, to detect the synchrotron emission from the accelerated electrons.

We found extended soft X-ray emission, suggesting a thermal plasma with $kT \sim 0.5$ keV both in the Suzaku and XMM spectra. Both the temperature and the projection profiles of the soft band images (figures 3 and 8) imply a close relationship between the soft emission and RCW 103. The best-fit $N_{\rm H}$ of 2–4 $\times 10^{21}\,{\rm cm^{-2}}$ in table 2 also support the connection, since these values are close to those obtained with the ASCA spectra (Gotthelf et al. 1997). The XMM-Newton profile (figure 8) suggests that it extends up to 15′ from the central point source, 1E 161348−5055, which is two-times as large as the radius of RCW 103. Although we cannot fully reject this possibility, at least for the Suzaku data, that this soft emission can be explained by an instrumental effect, the presence of this emission in the XMM-Newton data argues strongly for an astrophysical origin.

Many bright X-ray sources in the galactic plane have spatially extended X-ray halos, caused by the scattering of X-rays into our line of sight by interstellar dust between us and the object (Predehl, Schmitt 1995). The fact that the hard band profile of XMM-Newton does not extend beyond the rim of RCW 103 may support the dust halo hypothesis, since the scattering cross section ($\sigma_{\rm dust}$) depends strongly on the photon energy as $\sigma_{\rm dust} \propto E^{-2}$ (Predehl, Schmitt 1995). We will address the soft emission again in the future when the calibrations have become much robust. With careful work it may be possible to model the soft extended contamination over the region of HESS J1616 and further reduce the hard band X-ray flux limit.

5. Summary

We observed a bright TeV γ-ray object, HESS J1616, with the Suzaku XIS for 45 ks. There was no positive detection of hard X-ray emission, and we set an upper limit of $3.1 \times 10^{-13}\,{\rm erg\,s^{-1}\,cm^{-2}}$ to the 2–10 keV band flux. We also analyzed the XMM-Newton data of a 13 ks observation, and obtained a two-times higher upper limit of $6.9 \times 10^{-13}\,{\rm erg\,s^{-1}\,cm^{-2}}$. The deeper exposure and low background

performance of Suzaku explain this difference. The unusually high value of $f_{\rm TeV}/f_{\rm X} > 55$ makes HESS J1616 a very peculiar object. We also found diffuse X-rays consistent with thermal emission at $kT \sim 0.3$–$0.6\,$keV extending over this region from the SNR RCW 103. This emission is likely to be the result of scattering of X-rays from RCW 103 by interstellar dust.

The authors are grateful to Professors W. Hoffman and S. Funk for kindly providing the HESS image. We thank Professors H. Kunieda for his useful comments. We also thank all Suzaku members. This work is supported by a Grant-in-Aid for the 21st Century COE "Center for Diversity and Universality in Physics" from the Ministry of Education, Culture, Sports, Science and Technology (MEXT). HM is also supported by the MEXT, Grant-in-Aid for Young Scientists (B), 1874015, 2006. JPH acknowledges support from NASA grant NNG05GP87G.

References

Aharonian, F., et al. 2002, A&A, 393, L37
Aharonian, F., et al. 2004a, A&A, 425, L13
Aharonian, F., et al. 2005a, Science, 307, 1938
Aharonian, F., et al. 2005b, A&A, 435, L17
Aharonian, F., et al. 2005c, A&A, 437, L7
Aharonian, F., et al. 2006, ApJ, 636, 777
Aharonian, F. A., et al. 2004b, Nature, 432, 75
Anders, E., & Grevesse, N. 1989, Geochim. Cosmochim. Acta, 53, 197
Aschenbach, B., et al. 2000, Proc. SPIE, 4012, 731
Baganoff, F. K., et al. 2003, ApJ, 591, 891
Bamba, A., et al. 2007, PASJ, 59, S209
Bamba, A., Ueno, M., Koyama, K., & Yamauchi, S. 2003a, ApJ, 589, 253
Bamba, A., Yamazaki, R., Ueno, M., & Koyama, K. 2003b, ApJ, 589, 827
Bamba, A., Yamazaki, R., Yoshida, T., Terasawa, T., & Koyama, K. 2005, ApJ, 621, 793
Brogan, C. L., Gaensler, B. M., Gelfand, J. D., Lazendic, J. S., Lazio, T. J. W., Kassim, N. E., & McClure-Griffiths, N. M. 2005, ApJ, 629, L105
Butt, Y. M., et al. 2003, ApJ, 597, 494
Butt, Y. M., Drake, J., Benaglia, P., Combi, J. A., Dame, T., Miniati, F., & Romero, G. E. 2006, ApJ, 643, 238
Cheng, K. S., Taam, R. E., & Wang, W. 2004, ApJ, 617, 480
DeLaney, T., Gaensler, B. M., Arons, J., & Pivovaroff, M. J. 2006, ApJ, 640, 929
Fujimoto, R., et al. 2007, PASJ, 59, S133
Gotthelf, E. V., Petre, R., & Hwang, U. 1997, ApJ, 487, L175
Hwang, U., Decourchelle, A., Holt, S. S., & Petre, R. 2002, ApJ, 581, 1101
Ishisaki, Y., et al. 2007, PASJ, 59, S113
Kaneda, H., Makishima, K., Yamauchi, S., Koyama, K., Matsuzaki, K., & Yamasaki, N. Y. 1997, ApJ, 491, 638
Katagiri, H., et al. 2005, ApJ, 619, L163
Kokubun, M., et al. 2007, PASJ, 59, S53
Koyama, K., et al. 2007, PASJ, 59, S23
Koyama, K., Makishima, K., Tanaka, Y., & Tsunemi, H. 1986, PASJ, 38, 121
Koyama, K., Petre, R., Gotthelf, E. V., Hwang, U., Matsuura, M., Ozaki, M., & Holt, S. S. 1995, Nature, 378, 255
Landi, R., et al. 2006, ApJ, 651, 190
Lazendic, J. S., Slane, P. O., Gaensler, B. M., Reynolds, S. P., Plucinsky, P. P., & Hughes, J. P. 2004, ApJ, 602, 271
Mitsuda, K., et al. 2007, PASJ, 59, S1
Mori, H., et al. 2005, PASJ, 57, 245
Mukherjee, R., & Halpern, J. P. 2005, ApJ, 629, 1017
Mukherjee, R., Halpern, J. P., Gotthelf, E. V., Eracleous, M., & Mirabal, N. 2003, ApJ, 589, 487
Pannuti, T. G., Allen, G. E., Houck, J. C., & Sturner, S. J. 2003, ApJ, 593, 377
Predehl, P., & Schmitt, J. H. M. M. 1995, A&A, 293, 889
Revnivtsev, M., Sazonov, S., Gilfanov, M., Churazov, E., & Sunyaev, R. 2006, A&A, 452, 169
Rodriguez, J., Tomsick, J. A., Foschini, L., Walter, R., Goldwurm, A., Corbel, S., & Kaaret, P. 2003, A&A, 407, L41
Serlemitsos, P. J., et al. 2007, PASJ, 59, S9
Slane, P., Gaensler, B. M., Dame, T. M., Hughes, J. P., Plucinsky, P. P., & Green, A. 1999, ApJ, 525, 357
Slane, P., Hughes, J. P., Edgar, R. J., Plucinsky, P. P., Miyata, E., Tsunemi, H., & Aschenbach, B. 2001, ApJ, 548, 814
Smith, R. K., Brickhouse, N. S., Liedahl, D. A., & Raymond, J. C. 2001, ApJ, 556, L91
Strüder, L., et al. 2001, A&A, 365, L18
Sugizaki, M., Mitsuda, K., Kaneda, H., Matsuzaki, K., Yamauchi, S., & Koyama, K. 2001, ApJS, 134, 77
Takahashi, T., et al. 2007, PASJ, 59, S35
Torii, K., et al. 1998, ApJ, 494, L207
Tuohy, I., & Garmire, G. 1980, ApJ, 239, L107
Turner, M. J. L., et al. 2001, A&A, 365, L27
Ubertini, P., et al. 2005, ApJ, 629, L109
Vink, J., & Laming, J. M. 2003, ApJ, 584, 758
Worrall, D. M., Marshall, F. E., Boldt, E. A., & Swank, J. H. 1982, ApJ, 255, 111
Yamaguchi, H., et al. 2006, Proc. SPIE, 6266, 121
Yamauchi, S., & Koyama, K. 1993, ApJ, 404, 620
Yamazaki, R., Kohri, K., Bamba, A., Yoshida, T., Tsuribe, T., & Takahara, F. 2006, MNRAS, 371, 1975